Available online at www.sciencedirect.com
SCIENCE DIRECT®
Journal of Photochemistry and Photobiology A: Chemistry 166 (2004) 141–147
Journal of Photochemistry and Photobiology A:Chemistry
www.elsevier.com/locate/jphotochem

Photonic materials utilizing naturally occurring nanostructures

Hayato Kamioka [a,*], Hidenori Hiramatsu [a], Katsuro Hayashi [a], Masahiro Hirano [a], Hideo Hosono [a,b]

[a] *Hosono Transparent Electro-Active Materials Project, ERATO, Japan Science and Technology Agency, KSP C-1232, 3-2-1 Sakado, Takatsu-ku, Kawasaki 213-0012, Japan*
[b] *Materials and Structures Laboratory, Tokyo Institute of Technology, 4259 Nagatsuta, Midori-ku, Yokohama 226-8503, Japan*

Received 23 October 2003; received in revised form 4 December 2003; accepted 5 April 2004

Abstract

We report distinct optical/electrical properties inherent to build-in nanostructures in transparent oxide based materials, oxychalcogenides LaCuOS and LaCuOSe having naturally formed multi-quantum well structures and $12CaO{\cdot}7Al_2O_3$ (C12A7) with a unique nanoporous structure. LaCuOSe doped with Mg ions exhibit degenerative p-type conduction presumable due to "modulation doping mechanism" with a high mobility of 4.0 $cm^2\,V^{-1}\,s^{-1}$ even at high hole concentration ($\sim 2\times10^{20}\,cm^{-3}$). The room temperature exciton, having a large binding energy ($\sim$50 meV) due to the confinement effect of carriers in the CuS or CuSe layer, induces a large optical nonlinearity at room temperature (RT) ($\chi^{(3)} = 2$–4×10^{-9} esu) near the absorption band. The H^- ion entrapped in nanosize cages in C12A7 lattice causes an persistent conversion at RT from an electric insulator ($<10^{-10}\,S\,cm^{-1}$) to a semiconductor (0.3–100 $S\,cm^{-1}$) by capturing electrons photo-ionized from H^- ions in the cages. This is a first electronic conductor based on main group light metal oxides.

PACS: 42.65.Sf; 73.21.-b; 78.55.Mb; 78.67.-n; 82.45.Xy

Keywords: Nanostructure; LaCuOS; LaCuOSe; Exciton; Carrier confinement; C12A7; F^+ Center; Electronic conductor

1. Introduction

Oxide ceramics is probably among the oldest of man-made materials owing to the abundance and easy availability of the ingredients. Although most oxides are optically transparent, important for optical applications, it has been believed that active functions based on excited electrons, such as in crystalline semiconductor materials, are not possible. For example, alumina and glasses, which are representative oxides, are optically transparent but electrically insulating. If novel active functionalities utilizing both optical transparency and electron activity in oxide materials are realized, one can expect that a new frontier of materials science will be opened in front of us because these oxides are abundant and environmentally compatible. On the basis of this belief, we have focused on the band engineering and defect engineering for them in order to design an efficient electron-transfer system. It leads to the following our substantial results about transparent oxide semiconductors [1], nanoporous materials [2], optical oxides for vacuum/deep ultraviolet (UV) lasers [3], and nano-fabrication of transparent dielectrics by interfered femtosecond laser pulses [4].

In this paper we report our works on optical/photonic properties found in transparent materials based on oxides, which have build-in periodic nanostructures. Materials we focused on are LaCuOS, LaCuOSe and $12CaO{\cdot}7Al_2O_3$ (C12A7). LaCuOS and LaCuOSe is featured by two-dimensional layered structure, respectively composed of narrow-gap semiconductor Cu_2S and Cu_2Se sandwiched by wide gap insulator La_2O_3. This naturally occurring periodic nanolayers are not seen in typical compound semiconductors such as GaAs and GaN, and is a unique for oxides composed of a variety of chemical bonding nature. On the other hand, the C12A7 crystal has an exceptional nanoporous structure composed of positively charged lattice framework containing twelve cages and extra-framework oxygen ions occupying two different cages. This feature provides flexibility to replace the free oxygen ions with other anions by suitable thermal treatments. Thus, we can expect variety of novel electronic, optical and ionic properties appearing in C12A7 due to the incorporation of anions such as H^- and "electron" in the nano-sized cages. Several unique properties discovered in these materials such

* Corresponding author. Tel.: +81 44 850 9799; fax: +81 44 819 2205.
E-mail address: h-kamioka@net.ksp.or.jp (H. Kamioka).

1010-6030/$ – see front matter © 2004 Elsevier B.V. All rights reserved.
doi:10.1016/j.jphotochem.2004.04.033

as room temperature (RT) stable exciton, large optical nonlinearity and photo-induced insulator–conductor conversion are to be summarized, placing an emphasis on a crucial role of the nanostructures inherent to the crystal structures.

2. Oxychalcogenide: LaCuOCh with naturally formed layered structure

Transparent oxide semiconductors (TOS) are valuable materials that have both electrical conductivity and transparency in UV–vis light region. Almost all the TOS have n-type conductivity, and the TOS with p-type conductivity, required for valuable functionalities by PN junction, has seldom been to be realized. Oxychalcogenides LaCuOCh (Ch: chalcogen ion) compounds are exceptional TOS that combine wide bandgap with large p-type conductivity [5–7].

2.1. Crystal structure

The LaCuOCh have tetragonal system (space group: *P*4/*nmm*) with alternate layers of LaO and CuCh stacked along the *c*-axis as shown in Fig. 1 [8–10]. Each layer is constituted by edge-shared La_4O and $CuCh_4$ tetrahedra. Both S and Se can occupy the chalcogen site. Thus, there is a complete solid solution of LaCuOS–LaCuOSe system, i.e. $LaCuOS_{1-x}Se_x$ ($x = 0$–1) [5]. The La_2O_3 and Cu_2Ch, which basically composes the layered LaCuOCh, have bandgaps of ~5.5 eV and <2 eV, respectively. The density of state estimated from the energy band diagram for each layer in LaCuOCh reveals that this compound has a large band-offset feature. Therefore, we expect that these oxychalcogenides have quantum well structures naturally formed by their layered structures to exhibit quantum confinement effects.

2.2. Electrical properties

Fig. 2 shows hole transport properties of undoped (closed) and Mg 10 at.%-doped(open) $LaCuOS_{1-x}Se_x$ ($x = 0$–1) at 300 K. Hole concentration of undoped sample ($\sim 2\times10^{19}$ cm^{-3}) increases to $\sim 2\times10^{20}$ cm^{-3} by Mg doping. Hall mobility of the Mg-doped film increases from 0.2 to 4.0 cm^2 V^{-1} s^{-1} by replacing the anion S with Se, resulting in the increase in the electrical conductivity from 5.9 to 140 S cm^{-1}. The increase in the mobility is attributed to the enhancement of the valence band dispersion by the contribution of more extended Se 4p orbital. It would be worth noting that the mobility of the Mg-doped films is reduced only to half of that in the undoped films despite the heavy Mg ion doping. Coexistence of the large hole concentrations >10^{20} cm^{-3} and the moderately large mobility is unusual in conventional semiconductors. It may be attributed to the modulation doping based on the naturally formed layered crystal structure: i.e. Mg ion is doped in the LaO layer (carrier doping layer) and then the hole carriers generated in the layer are immediately transferred to the CuCh layer (hole conduction layer). Thus, the mobile hole carriers are not scattered by the charged impurities since the hole conduction layer is spatially separated from the doping layer, which naturally realizes the modulation doping structure such formed intentionally in a high electron mobility transistor (HEMT).

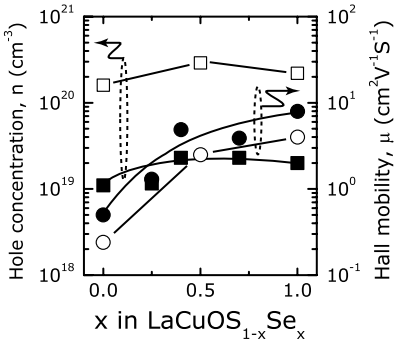

Fig. 2. Hole concentration (squares) and mobility (circles) of undoped (closed symbols) and 10-at.% Mg doped (open symbols) $LaCuOS_{1-x}Se_x$ ($x = 0$–1) at 300 K.

Fig. 3 shows temperature dependences of the hole concentration and the mobility for the Mg-doped LaCuOSe. The film exhibits p-type degenerate conduction with high hole concentrations >10^{20} cm^{-3}. This feature should be

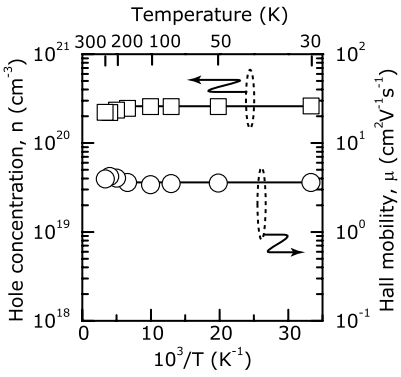

Fig. 3. Temperature dependence of hole concentration (squares) and Hall mobility (circles) of 10-at.% Mg doped LaCuOSe ($x = 1$).

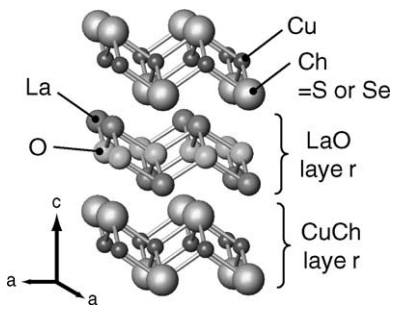

Fig. 1. Crystal structure of layered oxychalcogenides: LaCuOCh (Ch = chalcogen).

compared with conventional wide gap p-type semiconductors: maximum hole concentrations reported are $<10^{19}\,cm^{-3}$ for GaN:Mg or ZnSe:N, and they never show the degenerate conduction as their acceptor levels are deeper than 100 meV. This is a first demonstration of a p-type degenerate conduction in wide gap semiconductors [11,12].

2.3. Optical properties [13]

LaCuOS and LaCuOSe, which have wide bandgap energy due to the confinement of carriers in the CuS or CuSe layer, exhibit sharp photoluminescence (PL) and absorption bands around fundamental absorption region even at RT as shown in Fig. 4. The absorption spectrum of LaCuOS shows a single band at 3.2 eV. On the other hand, two absorption bands around 2.9 and 3.1 eV were observed in LaCuOSe. The calculation for energy band structure and symmetry analysis verify that the degenerated valence band maximum (VBM) is split into two singlet states due to the spin–orbit interaction of chalcogen ions [14]. The larger spin–orbit coupling in Se ion than in S ion causes the distinct splitting of absorption band in LaCuOSe. These absorption bands are attributed to band-edge excitons that are thermally stable even at RT due to the large binding energy.

The PL peak energies are located just below the absorption band due to excitons, which are in blue-UV light region [7,15]. Fig. 5 shows excitonic PL energy of the undoped $LaCuOS_{1-x}Se_x$ ($x = 0$–1) at 300 K as a function of a-axis length or chemical composition. The emission energy decreases almost linearly as a-axis length increases, which allows the emission energy tuning from 3.2 eV (390 nm) to 2.9 eV (430 nm) by changing the Se content, x. The decrease in the emission energy is attributed to the change in the VBM electronic structure. The substitution of S by Se causes an enhancement of VBM dispersion to result in the reduction of the energy bandgap. This kind of bandgap engineering should be quite effective for the fabrication of opto-electonic devices, especially for light-emitting diodes in terms of tuning emission wavelength.

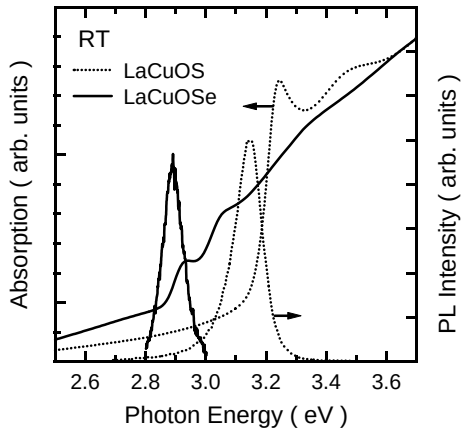

Fig. 4. PL and Absorption spectra for LaCuOS and LaCuOSe at RT.

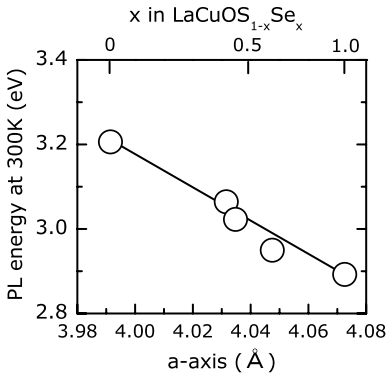

Fig. 5. PL peak energy of undoped $LaCuOS_{1-x}Se_x$ at 300 K as a function of the a-axis length or the Se content.

2.4. Nonlinear optical properties

The photo-excitation near the bandgap energy creates transiently generated excitons in the conductive CuS and CuSe layer. The studies for semiconductor quantum-well and nano-particle have revealed that the optical nonlinearity is highly enhanced at the resonant energy of the exciton, especially when the exciton has a large binding energy or is confined in the nanostructures [16,17]. The excitons with large binding energy are particularly favorable for practical applications because the enhancement takes place even at RT. Thus, it is expected that the confinement of the exciton in CuS and CuSe nano-layer also develop such a large optical nonlinearity in blue-UV light region. We confirmed the spectral intensity and time-response of the nonlinearity, represented by third-order optical susceptibility $\chi^{(3)}$, in the epitaxial thin films using a femtosecond time-resolved degenerative four-wave mixing (DFWM) technique around the bandgap energy at RT.

The DFWM measurements were carried out in a conventional pump-probe configuration. The second harmonic of a mode locked Ti:sapphire laser (tunable from 350 to 450 nm) with a pulse width of ~100 fs and repetition rate of 80 MHz was used as a light source. The pulse was split into two, which were chopped at different frequencies (f_1, f_2) and focused on the sample with a spot diameter of ~50 μm and a cross-angle of 8° between the pulse directions ($\boldsymbol{k}_1$ and $\boldsymbol{k}_2$). The excitation power density was 1.8×10^7 W/cm^2. The DFWM signal refracted in a forward direction $2\boldsymbol{k}_1$–$\boldsymbol{k}_2$ due to a transient grating formed in the sample was measured as a function of time delay between the split pulses using a photomultiplier connected to a lock-in amplifier synchronized at the sum frequency (f_1+f_2). The absolute values of $\chi^{(3)}$ for LaCuOS and LaCuOSe were determined by comparing the DFWM signal to the signal from a standard material (in this case, a silica glass plate) using a theoretical relation mentioned in a reference [18].

Fig. 6 shows the $\chi^{(3)}$ values of the epitaxial LaCuOS and LaCuOSe thin films as a function of excitation wavelength in the fundamental absorption region at RT, compared with

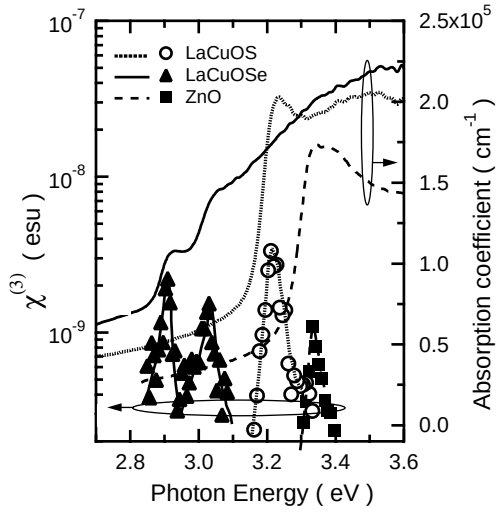

Fig. 6. $\chi^{(3)}$ and absorption spectra for LaCuOS, LaCuOSe and ZnO epitaxial thin films as a function of excitation energy. Measurement temperature: RT.

optical absorption spectra of the films. Those of the epitaxial ZnO film are also shown as a reference. The $\chi^{(3)}$ values for LaCuOS and LaCuOSe depend strongly on the excitation wavelength showing sharp peaks just below these absorption band peaks, which clearly indicates $\chi^{(3)}$ resonance with the exciton absorption. The $\chi^{(3)}$ values of the LaCuOS and LaCuOSe films are enhanced to $2–4\times10^{-9}$ esu at their absorption peaks, which is larger than that of the ZnO film (1×10^{-9} esu), while LaCuOS and LaCuOSe have smaller exciton binding energy (~50, 60 meV for ZnO). The larger $\chi^{(3)}$ values in LaCuOS and LaCuOSe presumably attribute to an increase in the density of exciton states caused by the exciton confinement in the CuS and CuSe layer [19]. These $\chi^{(3)}$ values are comparable with those for semiconductor CdS (or CdSe) nanoparticles dispersed in glass matrix.

The DFWM signals for LaCuOS and LaCuOSe as a function of the delay time between the pump and probe pulses are shown in Fig. 7. The excitation energies were fixed at the absorption band-edge peaks of LaCuOS and LaCuOSe,

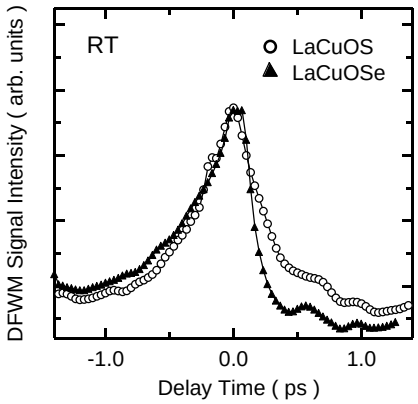

Fig. 7. DFWM signals as a function of time delay at the absorption peak energy of 3.2 eV for LaCuOS and of 2.9 eV for LaCuOSe.

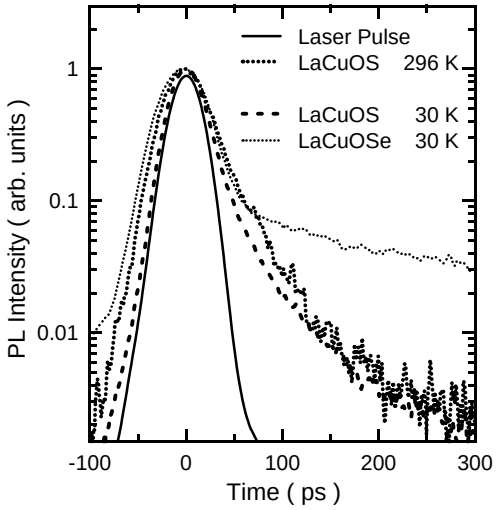

Fig. 8. Decay profiles of PL for LaCuOS and LaCuOSe at the peak energy.

respectively. The response times τ are ~250 and 300 fs for LaCuOS and Se at RT, respectively. On the other hand, Fig. 8 shows the normalized PL decay profiles of LaCuOS and LaCuOSe, which were measured using a streak camera with a picosecond time resolution at RT and 30 K. The third harmonic of a mode locked Ti:sapphire laser (center wavelength 870 nm) with a pulse width of ~100 fs and repetition rate of 1 kHz was used as an excitation light source. The energy decay times τ_1 of the excitons have been estimated as 30 ps for LaCuOS at RT and as 40 ps (200 ps) for LaCuOS (LaCuOSe) at 30 K through single exponential fittings for the photoluminescence decay curves. The decay time of LaCuOSe at RT cannot be obtained because of the weak PL intensity so far. The relatively slow decay of PL in LaCuOSe suggests that the photo-excited carrier transport to the lowest energy exciton after a retention at the upper energy exciton state before radiation. The large dissociation of τ from τ_1 in both samples reveals that the DFWM response time is not dominated by energy decay but rather the dephasing time τ_2 of the transient grating induced by nonlinear polarization from the intense laser pulse irradiation, as described by the relation $\tau = \tau_2/4$ in the exciton distribution with inhomogeneous broadening.

The $\chi^{(3)}$ resonance energy can be freely varied from 2.9 to 3.2 eV (380–420 nm) through the formation of solid solution for LaCuOS and LaCuOSe. This energy region just overlaps with the working area of GaN-based laser. That is, compound $LaCuOS_{1-x}Se_x$ ($x = 0–1$) is quite attractive for emerging applications such as an optical switching device operating in blue-UV light region.

3. Photo-induced conversion of from electronic insulator to conductor in C12A7

Main group light metal oxides, which are represented by alkaline-earth oxides, alumina, and silica, have been believed

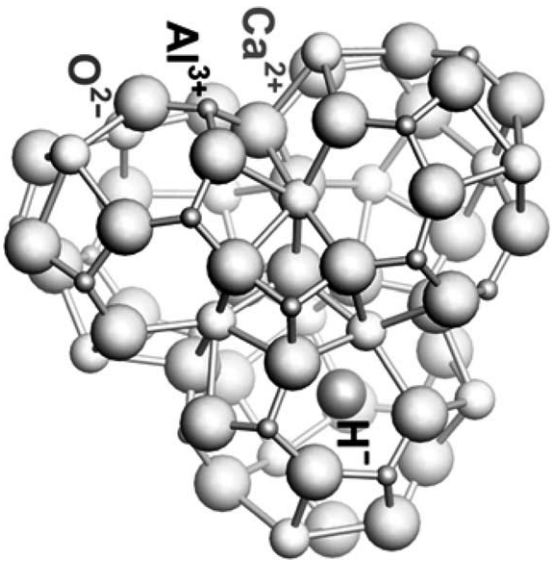

Fig. 9. Illustration of three neighboring cages in C12A7 extracted from the crystal lattice. One of the cages traps an H^- ion.

to be unexceptionally good insulators. By utilizing an inherent nanoporous structure, however, one of these classes of materials, C12A7, has been converted into an electronic conductor for the first time [20].

3.1. Incorporation of H-ion in nano-sized cage

The stoichiometric chemical formula for the unit cell ($Z = 2$) is represented as $[Ca_{24}Al_{28}O_{64}]^{4+} + 2O^{2-}$. The former denotes the lattice framework (lattice constant of 1.199 nm) including 12 cages with a free space of ~0.4 nm in diameter (Fig. 9) , thereby each cage has a mean effective charge of +1/3 (= +4 /12) [21]. The latter is called 'free oxygen ion', which is loosely bound in the cage and compensates for the positively charged framework. These features provide flexibility for substituting other anions such as OH^- [22], F^-, Cl^- [23], O^{2-} [24–26] and O^- [25,26] for the free oxygen ion.

A thermal treatment in hydrogen atmosphere (e.g. 1300 °C, 20% H_2–80% N_2) incorporates hydride ion, H^-, into the cage. Analysis by nuclear magnetic resonance (NMR), secondary ion mass spectroscopy (SIMS), and infrared absorption spectroscopy revealed that C12A7 after the treatment contains high concentration (2×10^{20} cm^{-3}) of the H^- ion. Presence of the H^- ion is supported by the release of hydrogen molecules at 500–750 °C (Fig. 10a) when heated in He gas.

3.2. Optical and electrical properties

The H^--loaded C12A7 (C12A7:H) single-crystal looks colorless transparent (Fig. 11) and a good insulator having electric conductivity $<10^{-10}$ S cm^{-1}. However, illumination of UV light changed the color from transparent to yellowish green due to the emergence of optical absorption bands at 2.8 and 0.4 eV. Even after the illumination was stopped, these absorptions remained unchanged. Fig. 11 also plots the relative efficiency of the color center yield as a function of the photon energy in the irradiated light. The optical absorption edge of intrinsic C12A7 crystal locates at ~5 eV and shifted to ~4 eV by the H^- incorporation. An agreement of the maximum efficiency (~4.1 eV) with the absorption edge indicates that the photo-excitation of the H^- ion is responsible for the coloration. Simultaneously with the coloration,

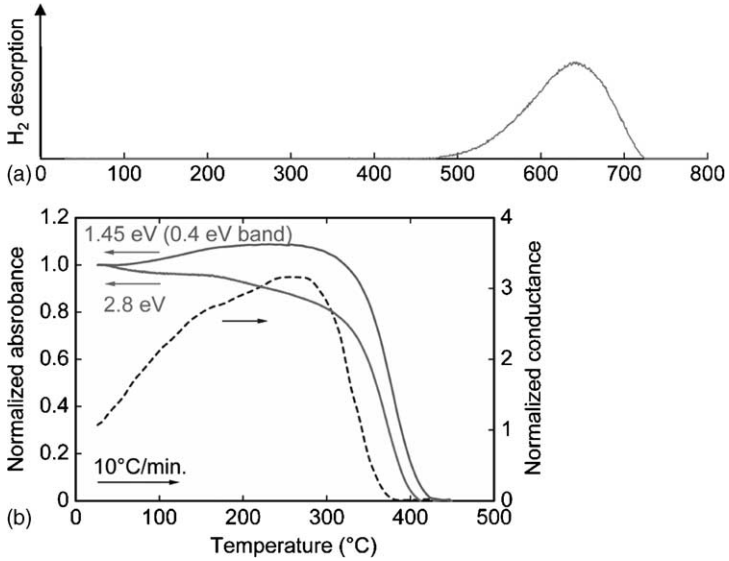

Fig. 10. Thermal changes in C12A7:H or UV-irradiated C12A7:H. (a) Thermogravimetric-mass spectroscopy (TG-MS) analysis on C12A7:H. Polycrystalline C12A7:H was heated at a rate of 10 K min^{-1} in a He atmosphere. Intensity of H_2 ($m/e = 2$) desorption was recorded. (b) The decay of the absorbance at 2.8 and 1.5 eV (as a measure of the 0.4 eV band) and conductance upon heating. The C12A7 sample was illuminated by Xe-lamp light for 15 min prior to the heating.

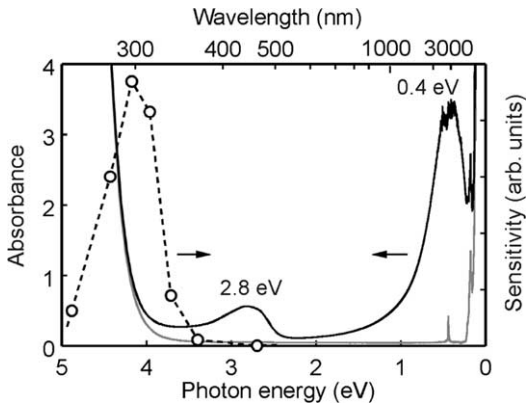

Fig. 11. The absorption spectra of C12A7:H single-crystals (0.3 mm thick) before (gray solid line) and after (black solid line) illuminating with UV radiation (4.9 eV light to 2×10^{20} photons cm^{-2}). The sensitivity of the light-induced coloration is plotted by circles. The inset is a photo of C12A7:H single crystals ($2.8\times2.8\times0.3'$ mm^3) before (left) and after (right) UV-light illumination.

the electric conductivity increased drastically to 0.3 S cm^{-1} at 300 K. This value is at least a billion times greater than that before the UV irradiation.

Since an electron paramagnetic resonance (EPR) signal with an isotropic Lorenzian shape was observed at $g = 1.994$ upon the irradiation, the two optical absorption bands are attributed to an F^+-like center [27], which is created by an electron trapping in the cage. The UV-irradiation, therefore, is considered to induce an electron emission from the H^- ions ($H^- \rightarrow H_0 + e^-$). Then, an empty cage captures the electron, forming the F^+-like center. Further, a migration of the electrons at the F^+-like centers may be responsible for the electronic conduction. These observations were confirmed by an ab initio calculation [28]. The results of calculation demonstrated that the electron could be localized at the center of the cage with s-character. However, a small barrier (~0.1–0.2 eV) for inter-cage hopping of the electron assisted by a strong lattice relaxation allows a polaronic electronic transportation. Further, the 0.4 eV band is interpreted as the inter-cage s → s transition, while 2.8 eV band is assigned to the intra-cage s → p transitions.

As shown in Fig. 10b, the inversion to the insulator occurred accompanying with the rapid decay of the optical absorptions when heated >300 °C. Further heating >550 °C caused the release of H_2 gas from the C12A7:H as in Fig. 10a, and then, the photosensitivity got lost. In other words, the emergence of the insulator–conductor conversion is reversible unless the heating temperature is high enough to release the H^- ion.

The present properties provide novel applications like a direct patterning of transparent electronic circuits by the UV-light. Thin film having such function was realized by the pulsed laser deposition followed by a high-temperature (1200 °C) hydrogen annealing [29]. Further, an H_2^+ ion implantation was also demonstrated to form the H^- ion in C12A7 [30]. This technique makes it possible to lower the process temperature to 500–700 °C and to control the electrical conductivity easily. In addition, it is noteworthy that high electronic conductivity exceeding 100 S cm^{-1} at 300 K was recently attained by a complete substitution of the free oxygen ions with electrons [31]. The resulting C12A7 is regarded as a thermally and chemically stable ‘electride’ [32].

4. Summary

We have briefly reported our recent works preformed in “Transparent Electro Active Materials Project”, placing emphases on optical/electrical properties inherent to build-in nanostructures in transparent materials based on oxides. Materials we focused on are oxychalcogenides LaCuOS and LaCuOSe, having naturally formed multi-quantum well structures, and $12CaO{\cdot}7Al_2O_3$ (C12A7) with a unique nanoporous structure.

The room temperature excitons in LaCuOS, which has a large binding energy due to the confinement effect of carriers in the CuS, shift to lower energy side with the substitution of S with Se ions, accompanied with the splitting due to the larger spin–orbit interaction of Se ion. The third order optical susceptibilities, measured by a femtosecond time-resolved degenerative four wave mixing technique, depend strongly on wavelength, showing sharp resonance peaks to the exciton absorption bands. The $\chi^{(3)}$ values at room temperature reach $2–4\times10^{-9}$ esu, which are larger than that of ZnO presumably due to the confinement of the exciton in the CuS and CuSe layer. Further, the degenerative conduction is realized in Mg doped LaCuOSe for the first time among wide gap p-type semiconductors. The modulation doping mechanism likely works in the system, where Mg ions occupy La sites in the LaO layer and the generated carriers move in the CuS and CuSe layer. Such spatial separation between the doping site and the conduction path keeps the hole mobility remarkably larger and makes the hole concentration higher, leading to the degenerate conduction.

Under the thermal treatment in hydrogen atmosphere, C12A7 incorporates H^- ions in the nano-sized cages embedded in the lattice framework. The obtained H^--loaded C12A7 undergoes an persistent conversion at room temperature from the electric insulator to semiconductor, accompanied with coloration from transparent to yellowish green with an irradiation of UV light. The empty cages capture the photo-released electrons from the H^- ions to form F^+ like centers. The electrons are so loosely bound to the cages that they can migrate among cages, causing the electric conductivity. This is the first example for the main group oxide to exhibit electric conductivity. The photo-induced process is practically useful for writing electric wiring patterns by light.

These examples described in this paper demonstrate realization of excellent photonic features in oxide-based materials applicable for emerging devices. These features are

derived from their natural occurring nanostructures, which never exist in typical compound semiconductors. Present attainments open a new frontier of material science, paving a way to "invisible oxide electronics".

Acknowledgements

This work was achieved in the research project called "Transparent Electro-Active Materials (TEAM)" from October 1999 (to September 2004) within a framework of Exploratory Research for Advanced Technology (ERATO) under the sponsorship of Japan Science and Technology Agency (JST). The purpose of this project is to cultivate the new frontier of transparent oxides as functional materials by exploring novel active properties based on excited electrons.

References

[1] H. Hosono, H. Ohta, M. Orita, K. Ueda, M. Hirano, Vacuum 66 (2002) 19;
K. Nomura, H. Ohta, K. Ueda, T. Kamiya, M. Hirano, H. Hosono, Science 300 (2003) 1269.
[2] H. Hosono, Solid-State Phys. 38 (2003) 423.
[3] H. Hosono, Y. Ikuta, T. Kinoshita, K. Kajihara, M. Hirano, Phys. Rev. Lett. 87 (2001) 175501;
M. Oto, S. Kikugawa, N. Sarukura, M. Hirano, H. Hosono, IEEE Photon. Technol. Lett. 13 (2001) 978.
[4] K. Kawamura, N. Ito, N. Sarukura, M. Hirano, H. Hosono, Rev. Sci. Instrum. 73 (2002) 1711;
K. Kawamura, T. Kamiya, M. Hirano, H. Hosono, Appl. Phys. Lett. 81 (2002) 1137.
[5] K. Ueda, H. Hosono, J. Appl. Phys. 91 (2002) 4768.
[6] K. Ueda, S. Inoue, S. Hirose, H. Kawazoe, H. Hosono, Appl. Phys. Lett. 77 (2000) 2701.
[7] K. Ueda, K. Takafuji, H. Hiramatsu, H. Ohta, T. Kamiya, M. Hirano, H. Hosono, Chem. Mater. 15 (2003) 3692.
[8] M. Palazzi, C. Carcaly, J. Flahaut, J. Solid-State Chem. 35 (1980) 150.
[9] W.J. Zhu, Y.Z. Huang, C. Dong, Z.X. Zhao, Mater. Res. Bull. 29 (1994) 143.
[10] D.O. Charkin, A.V. Akopyan, V.A. Dolgikh, Russ. J. Inorg. Chem. 44 (1999) 833.
[11] H. Hiramatsu, K. Ueda, H. Ohta, M. Hirano, T. Kamiya, H. Hosono, Appl. Phys. Lett. 82 (2003) 1048.
[12] H. Hiramatsu, K. Ueda, H. Ohta, M. Hirano, T. Kamiya, H. Hosono, Thin Solid Films 445 (2003) 304.
[13] H. Hiramatsu, K. Ueda, K. Takafuji, H. Ohta, M. Hirano, T. Kamiya, H. Hosono, J. Appl. Phys. 94 (2003) 5805.
[14] K. Ueda, H. Hiramatsu, H. Ohta, M. Hirano, T. Kamiya, H. Hosono, Phys. Rev. B 69 (2004) 155305.
[15] K. Ueda, S. Inoue, H. Hosono, N. Sarukura, M. Hirano, Appl. Phys. Lett. 78 (2001) 2333.
[16] Y. Li, M. Tanaka, A. Nakamura, Phys. Rev. B 57 (1998) 9193.
[17] D.S. Chemla, D.A.B. Miller, J. Opt. Soc. Am. B 2 (1985) 1155.
[18] R.L. Sutherland, Handbook of Nonlinear Optics, Marcel Dekker, NewYork, 1996.
[19] H. Kamioka, H. Hiramatsu, H. Ohta, M. Hirano, K. Ueda, T. Kamiya, H. Hosono, Appl. Phys. Lett. 84 (2004) 879.
[20] K. Hayashi, S. Matsuishi, T. Kamiya, M. Hirano, H. Hosono, Nature 419 (2002) 462.
[21] H. Bartl, T. Scheller, N. Jb. Miner. Mh. 35 (1970) 547.
[22] J.A. Imlach, L.S.D. Glasser, F.P. Glasser, Cement Conc. Res. 1 (1971) 57.
[23] J. Jeevaratnam, F.P. Glasser, L.S.D. Glasser, J. Am. Ceram. Soc. 47 (1964) 105.
[24] H. Hosono, Y. Abe, Inorg. Chem. 26 (1987) 1192.
[25] K. Hayashi, M. Hirano, S. Matsuishi, H. Hosono, J. Am. Chem. Soc. 124 (2002) 738.
[26] K. Hayashi, S. Matsuishi, N. Ueda, M. Hirano, H. Hosono, Chem. Mater. 15 (2003) 1851.
[27] F. Agullo-Lopez, C.R.A. Catlow, P.D. Townsend, Point Defects in Materials, Academic Press, London, 1988 (Chapter 5).
[28] P.V. Sushko, A.L. Shulger, K. Hayashi, M. Hirano, H. Hosono, Phys. Rev. Lett. 91 (2003) 126401.
[29] Y. Toda, M. Miyakawa, K. Hayashi, T. Kamiya, M. Hirano, H. Hosono, Thin Solid Films 445 (2004) 309.
[30] H. Miyakawa, K. Hayashi, M. Hirano, Y. Toda, T. Kamiya, H. Hosono, Adv. Mater. 15 (2003) 1100.
[31] S. Matsuishi, Y. Toda, M. Miyakawa, K. Hayashi, T. Kamiya, M. Hirano, I. Tanaka, H. Hosono, Science 301 (2003) 626.
[32] J.L. Dye, Inorg. Chem. 36 (1997) 3817.